ow in 3-d compressible porous media in the presence of multiple line sources and sinks are presented for examples with $h=l$ $1=40$; results in (4), for single-phase uid ow in two-dimensional (2-d) axisymmetric and anisotropic porous media, are presented for examples with $h=l$ $1=500$.

Whereas for standard numerical schemes this small aspect ratio can be problematical, here we present an approach based on matched asymptotic expansions in $h=l$ 1 (de ned explicitly in (2.10) below) for which the accuracy improves as

$$v = \quad D_y(x;y;z)\frac{@p}{@y}; \tag{2:3}$$

$$^2w = \quad D_z(x;y;z)\frac{@p}{@z}; \tag{2:4}$$

for $(x;y;z)$ 2 M^0, t 2 $(0;1)$, whose solution we will study in this paper. Here $(x;y;z)$ are rectangular ccy7esian coordina7es with z pointing vertically upwards, and the dimensionless domain is

$$M^0 = f(x;y;z)\ 2\ \mathbb{R}^3 : (x;y)\ 2 \quad ; z\ 2\ (z \quad (x;y); z_+(x;y))g; \tag{2.5}$$

with closure $\overline{M}^0$ and boundary $@M$ y xy @Mz 98 1287 6.5738 Tf: Tf -0.846 0 Td [(p)]T1751 9d [/F1 1 149.815 595.649 cm []0 d permeability scales (divided by constant uid velocity) in the horizontal and vertical directions respectively. Our matched asymptotic approach will rely on the assumption that 1. This is often the case in practice, with oil and gas reservoirs typically extending many orders of magnitude further horizontally compared to their depth.

The boundary conditions are, in dimensionless form,

$$(u(\mathrm{r};t);v(\mathrm{r};t);w(\mathrm{r};t)) \quad \hat{n} = 0; \quad \text{for all } (\mathrm{r};t) \in \partial M^0_H \quad (0;\infty); \tag{2:11}$$

$$w(\mathrm{r};t) \quad \frac{\partial z_+}{\partial x}(x;y)u(\mathrm{r};t)+\frac{\partial z_+}{\partial y}(x;y)v(\mathrm{r};t) \quad = 0; \text{ for all } (\mathrm{r};t) \in \partial M^0_+ \quad (0;\infty); \tag{2:12}$$

$$w(\mathrm{r};t) \quad \frac{\partial z}{\partial x}(x;y)u(\mathrm{r};t)+\frac{\partial z}{\partial y}(x;y)v(\mathrm{r};t) \quad = 0; \text{ for all } (\mathrm{r};t) \in \partial M^0 \quad (0;\infty); \tag{2:13}$$

where $\hat{n}(x;y)$ for $(x;y) \in \partial$ represents the outward unit normal eld to ∂ , ∂M^0_H ∂M^0 is that part of ∂M^0 representing the side walls of the boundary, $\partial M^0_+;\partial M^0$ ∂M^0 represent the upper and lower surfaces of ∂M^0 respectively, with $\partial M^0_+ \cup \partial M^0 \cup \partial M^0_H = \partial M^0$, and r := (

++

for all (r; t) $2\ \overline{M}^{0}$ [0; 1), where the constant $\hat{}_T$, representing the weighted dimensionless net ux of uid into or out of the porous layer, is given by

$$\hat{}_T = \frac{1}{\ldots}$$

for all r 2 $\overline{M}^0$. It follows [(.)-444(It)-330 m 10.751 0 l S Q BT /F11 9.9626 Tf 141.891 694.174 Td [(M)]Tn).826)

2.1 *Solution to [PSSP]*

It is shown in (**6**, x3) that the outer region asymptotic expansions (away from the sources/sinks) are given by

$$\hat{p}(\mathbf{r};\ ) = A(x;y) + O(\ ^2); \tag{2:37}$$

$$\hat{u}(\mathbf{r};\ ) = D_x(x;y;z)\frac{@A}{@x}(x;y) + O(\ ^2); \tag{2:38}$$

$$\hat{v}(\mathbf{r};\ ) = D_y$$

It follows from (2.7) and (2.20) that

$$\iint F(x,y)\,\mathrm{d}x\,\mathrm{d}y = 0, \tag{2.44}$$

and hence by classical theory for strongly elliptic boundary value problems (see for example (9)) that [BVP] has a unique solution. In particular, with $A : \bar{\ } \mapsto \mathbb{R}$ being the solution to [BVP], it is shown in (6, equation (3.18)) that

$$A(x,y) = \frac{{}_i}{4\ (D_x^i D_y^i)^{\frac{1}{2}}} \log \left[\frac{(x - x_i)^2}{D_x^i} + \frac{(y - y_i)^2}{D_y^i} \right] + A_0^i + O\left(([x - x_i]^2 + [y - y_i]^2)^{\frac{1}{2}} \right); \tag{2.45}$$

as $(x,y) \to (x_i,y_i)$, with $A_0^i \in \mathbb{R}$ being a globally determined constant and $D_x^i = D_x(x_i,y_i)$, $D_y^i = D_y(x_i,y_i)$, for $i = 1,\dots,N$.

In general, except for particularly simple boundaries ∂ , permeabilities D_x, D_y, and line source/sink locations $(x_i,y_i) \in \partial$, $i = 1,\dots,N$, [BVP] will need to be solved numerically. However, [BVP] is a 2-d, regular, strongly elliptic problem, and numerical solution via finite element methods can be achieved rapidly and accurately. We defer detailed consideration of the numerical solution of [BVP] until §3.1.

It is shown in (6) that the outer region asymptotic expansions (2.37)–(2.40) become non-uniform when $r \in {}_i$ as $\to 0$ ($i = 1,\dots,N$). To obtain a uniform asymptotic representation of the solution to [PSSP] when $r \in {}_i$ as $\to 0$, we must therefore introduce an inner region at each line source/sink location $(x,y) = (x_i,y_i)$, $i = 1,\dots,N$. In the inner region we write $(x,y) = (x_i,y_i) + (X,Y)$, with (X,Y) D_x,8d.01d [(x)]TJ8738 [(;)-167(y)]T4193 Td [(as)]TJ2.e-2.519 Td [(D)]T4 9 eigenfunctions of the regular Sturm-Liouville eigenvalue problem,

$$\left(D_z(z)\ {}'(z)\right)' + \ D_h(z)\ (z) = 0; \quad z \in (z^i\ ; z^i_+); \tag{2.48}$$

$$'(z^i\ ) = \ '(z^i_+) = 0; \tag{2.49}$$

which we refer to as [SL]. The eigenvalues of [SL] have $0 = \ _0 < \ _1 < \ _2 < \ldots$, (see e.g. (11, chapters 7,8)) with $\ _r \to \infty$ as $r \to \infty$, and the corresponding eigenfunctions are normalised so that

$$\langle\ _j ; \ _k\rangle = \int_{z^i_-}^{z^i_+} D_h(s)\ _j(s)\ _k(s)\,\mathrm{d}s = \ _{jk}; \tag{2.50}$$

for $j; k = 0; 1; 2; \ldots$. The constants B_r, $r = 1; 2; \ldots$ are given by

$$B_r = \frac{1}{2}\int_{z^i_-}^{z^i_+} s_i(\ )\ _r(\ )\,\mathrm{d}\ ; \quad r = 1; 2; \ldots : \tag{2.51}$$

~ 1

The asymptotic expansions for the ow elds $\hat{u}$, $\hat{v}$, $\hat{w}$ in the inner region are then given by

$$\hat{u}(X; Y; z; \ ) = \ ^1\left(D_x(z)\frac{X}{R_i}\left(\frac{\ _i}{2\ D^i_h R_i} \sum_{j=1}^{\infty} B_j\ ^{1/2}_j K_1(\ ^{1/2}_j R_i)\ _j(z)\right) + O(\ )\right); (2A$$

(zX in te6 1 9.9626 Tf 8.302 D^2_{xz} j 1

(vii) Compute the transient pressure $\tilde{p}$, given by (2.59), via computation of the coefficients c_r, $r = 1, 2, \ldots$, given by (2.60)–(2.61);

(viii) Compute the approximations to the dimensionless fluid pressure and velocity fields, given by (2.16)–(2.19) and (2.6).

We outline the implementation (used to generate the numerical results of §4) for each of these steps in §§3.1–3.8.

3.1 *Numerical solution of [BVP]*

To solve [BVP], given by (2.41)–(2.43), we use a standard finite element method, with a piecewise linear approximation space on a quasi-uniform triangulation of the 2-d domain Ω. There is a very wide literature on the efficient implementation of finite element methods for the solution of elliptic problems such as this (see e.g. (13, 14)), but we provide some brief details here both for completeness and also to ease the explanation of the implementation details provided in §§3.2–3.8.

A weak formulation of (2.41)–(2.42) is: Find $A \in H^1(\Omega)$ such that

$$\int_{\Omega} D_x \frac{\partial A}{\partial x}\frac{\partial v}{\partial x} + D_y$$

gives us

$$\sum_{j=1}^{N_e} u_j \iint_\Omega \hat{\phi}(x,y)\,\phi_j(x,y)\,\mathrm{d}x\,\mathrm{d}y = I_0.$$

Applying this immediately to (3.3) would lead to an overdetermined system, so to avoid this we add $\lambda \iint_\Omega \hat{\phi}(x,y)\,\phi_m(x,y)\,\mathrm{d}x\,\mathrm{d}y$ to the left hand side of (3.3) for each $m = 1,\dots,N_e$, to give a uniquely solvable $(N_e+1)\times(N_e+1)$ linear system for the unknowns u_j, $j = 1,\dots,N_e$ and λ, with $\lambda = 0$ returning (3.3) exactly. More specifically, we define the matrix $K = [K_{m,j}]$ $j,m = 1,\dots,N_e$ by

$$K_{m,j} = \int_\Omega \left(D_x \frac{\partial \phi_j}{\partial x}\frac{\partial \phi_m}{\partial x} + D_y \frac{\partial \phi_j}{\partial y}\frac{\partial \phi_m}{\partial y} \right) \mathrm{d}\Omega, \quad j,m = 1,\dots,N_e, \tag{3.4}$$

the vector $\mathbf{f} = [f_1 \dots f_{N_e}]^T$ by

$$f_m = \sum_{i=1}^{N} \beta_i\,\phi_m(x_i,y_i) - \hat{\phi}_T \iint_\Omega \hat{\phi}(x,y)\,\phi_m(x,y)\,\mathrm{d}x\,\mathrm{d}y, \quad m = 1,\dots,N_e, \tag{3.5}$$

the vector $\mathbf{b} = [b_1 \dots b_{N_e}]^T$ by

$$b_m = \iint_\Omega \hat{\phi}(x,y)\,\phi_m(x,y)\,\mathrm{d}x\,\mathrm{d}y, \quad m = 1,\dots,N_e, \tag{3.6}$$

and we take $\mathbf{u} = [u_1 \dots u_{N_e}]^T$. The linear system that we solve for the unknown coefficients u_j, $j = 1,\dots,N_e$, of (3.2) is then

$$\begin{pmatrix} K & \mathbf{b} \\ \mathbf{b}^T & 0 \end{pmatrix} \begin{pmatrix} \mathbf{u} \\ \lambda \end{pmatrix} = \begin{pmatrix} \mathbf{f} \\ I_0 \end{pmatrix}. \tag{3.7}$$

To evaluate meas($\overline{M}^{0}$

initial pressure variation is given by the final solution from a previous run (if one wishes to consider the effect of varying production rates, for example, see §4), then the integration scheme outlined above may not be sufficiently accurate. In this case, a better approach would be to use a partition of unity to split the integral, so that the inner and outer regions can be considered separately, with the approach described above being appropriate for the outer region, and a more suitable graded mesh being used on each inner region in order to deal with the singular behaviour of the solution near the line sources/sinks. This is the approach used to compute the constants c_r, defined by (2.60), arising in the series representation for the transient pressure field $\tilde{p}$, given by (2.59), and full details are provided in §3.7 below.

3.2 *Computation of outer region asymptotic expansions*

Having solved [BVP], we are now in a position to construct the outer region asymptotic expansions, accurate to $O(\epsilon^2)$, given by (2.37)–(2.40), that is,

$$\begin{aligned}
\hat{p}(x,y,z,\tau) &\sim A(x,y), \qquad\qquad (3.9)\\
\hat{u}(x,y,z,\tau) &\sim -D_x(x,y,z)\frac{\partial A}{\partial x}(x,y),\\
\hat{v}(x,y,z,\tau) &\sim -D_y(x,y,z)\frac{\partial A}{\partial y}(x,y),\\
\hat{w}(x,y,z,\tau) &\sim \int_{z_-(x,y)}^{z}\left[\frac{\partial}{\partial x}\left(D_x(x,y,\zeta)\frac{\partial A}{\partial x}(x,y)\right)+\frac{\partial}{\partial y}\left(D_y(x,y,\zeta)\frac{\partial A}{\partial y}(x,y)\right)\right]d\zeta\\
&\quad-\hat{\lambda}_T\int_{z_-(x,y)}^{z}\phi(x,y,\zeta)\,d\zeta.
\end{aligned}$$

The approximation to the pseudo-steady state pressure field on the outer region, $\hat{p}$, follows immediately from our approximation to $A(x,y)$, but to find $\hat{u}$, $\hat{v}$ and $\hat{w}$ we need to do a bit more work.

To approximate $\hat{u}$, rather than differentiating the function $A(x,y)$ explicitly (which would lead to a piecewise constant approximation, discontinuous across element boundaries), we instead write $\hat{u}(x,y,z,\tau) \sim \sum_{i=1}^{N_e}\hat{u}_i(z,\tau)\phi_i(x,y)$, and determine the functions $\hat{u}_i(z,\tau)$ (which will provide an approximation to $\hat{u}(x_i,y_i,z,\tau)$) by solving a weak form of

$$\sum_{i=1}^{N_e}\hat{u}_i(z,\tau)\phi_i(x,y) = -D_x(x,y,z)\frac{\partial A}{\partial x}(x,y),$$

specifically (recalling (3.2))

$$\sum_{i=1}^{N_e}\hat{u}_i(z,\tau)\iint_{\Omega}\phi_i(x,y)\phi_m(x,y)\,dx\,dy = -\sum_{j=1}^{N_e}u_j\iint_{\Omega}D_x(x,y,z)\frac{\partial\phi_j(x,y)}{\partial x}\phi_m(x,y)\,dx\,dy, \tag{3.10}$$

for $m = 1,\ldots,N_e$. To determine $\hat{u}_i(z,\tau)$, $i = 1,\ldots,N_e$, from (3.10), we use a form of mass lumping. We define $I^h : C(\bar{\Omega}) \mapsto S^h$ to be the linear interpolation operator from the space of continuous functions on $\bar{\Omega}$ to the space of functions that are linear on each triangle

$_i$, so that for $v \in C(\Gamma)$, $^h v(x_j; y_j$

$j = 1, \ldots, M_{SL}$, with $\tilde{\phi}_j(\bar{z}_m) = \delta_{jm}$. We then replace ϕ in (3.13) with ϕ^M defined by

$$\phi^M(z) = \sum_{j=0}^{M_{SL}} \tilde{\phi}_j(z)\, \phi^M(\bar{z}_j); \tag{3.14}$$

and require this equation to hold for each $\tilde{\phi} = \tilde{\phi}_m$, $m = 0, \ldots, M_{SL}$, leading to the linear system

$$\bar{K}\mathbf{v} = \lambda \bar{M}\mathbf{v}; \tag{3.15}$$

where $\mathbf{v} = [\phi^M(\bar{z}_0) \ldots \phi^M(\bar{z}_{M_{SL}})]^T$, $\bar{K} = [\bar{K}_{m,j}]$ and $\bar{M} = [\bar{M}_{m,j}]$, $j, m = 0, \ldots, M_{SL}$, with

$$\bar{K}_{m,j} = \int_{z_-^i}^{z_+^i} D_z(z)\tilde{\phi}_j'(z)\tilde{\phi}_m'(z)\,\mathrm{d}z; \quad j, m = 0, \ldots, M_{SL}; \tag{3.16}$$

$$\bar{M}_{m,j} = \int_{z_-^i}^{z_+^i} D_h(z)\tilde{\phi}_j(z)\tilde{\phi}_m(z)\,\mathrm{d}z; \quad j, m = 0, \ldots, M_{SL}. \tag{3.17}$$

The matrix $\bar{K}$ is tridiagonal, and for the results of §4 we evaluate the integrals (3.16) using the trapezoidal rule with $\bar{z}_j$, $j = 0, \ldots, M_{SL}$ as the nodes. To evaluate $\bar{M}$ we use an analogous procedure to that described in §3.2 of replacing the integrand in (3.17) by its piecewise linear interpolant, which leads to a diagonal matrix. The first few eigenvalues of [SL] are then approximated by the first few eigenvalues of $\bar{M}^{-1}\bar{K}$, and the eigenfunctions of [SL] are approximated using (3.14) with $\mathbf{v}$ the corresponding eigenvectors of $\bar{M}^{-1}\bar{K}$. It then just remains to normalise the eigenfunctions, using (2.50). Given an eigenfunction ϕ^M, the normalised eigenfunction is given by

$$\tilde{\phi}^M = \frac{\phi^M}{\sqrt{\qquad}}$$

To approximate the integral in the denominator on the right hand side of (3.23) we use the same procedure applied in (3.22), i.e. we replace the integrand by its piecewise linear interpolant on the triangulation of $\bar{\Omega}$. This allows us to reuse some of the computations required in the setting up of the mass matrix for $[\mathrm{EVP}]'$. Specifically, recalling (3.21), we have

$$\iint_{\Omega} \hat{\rho}(x,y)[\tilde{A}(x,y)]^2 \, \mathrm{d}x \, \mathrm{d}y \approx \iint_{\Omega_h} \left\{ \hat{\rho}(x,y) \left(\sum_{j=1}^{N_e} \tilde{a}_j \phi_j(x,y) \right)^2 \right\} \mathrm{d}x \, \mathrm{d}y$$

$$= \sum_{j=1}^{N_e} \tilde{a}_j^2 \, \hat{\rho}(\tilde{x}_j, \tilde{y}_j) \iint_{\Omega} \phi_j(x,y) \, \mathrm{d}x \, \mathrm{d}y .$$

Comparing with (3.22) it is clear that the integral in the denominator on the right hand side of (3.23) can be computed with only a very small number of additional calculations.

3.7 *Computation of transient pressure $\tilde{p}$*

Having solved [EVP]

of I_1 being appropriate for the outer region, and a more suitable graded mesh being used to evaluate the integrals on the inner region in order to deal with the singular behaviour there. Speci cally, we choose constants $0 < a < b$, where $a; b = O( )$, and we write $I_2 = \sum_{j=1}^{N+1} I_2^j$, where for j

4. Numerical examples

For all of the examples in this section $\overline{M}^{0}$ is given by (2.5), with Ω the ellipse $\Omega = \{(x,y) : x^2 + 4y^2 < 1\}$, and the variable upper and lower boundaries given by

$$z_+(x,y) = \frac{1}{2}(x^2+4y^2) + \frac{1}{2}, \quad \text{and} \quad z_-(x,y) = -\frac{1}{2}(x^2+4y^2) - \frac{1}{2},$$

for $x, y \in \overline{\Omega}$. The permeability of the layer is nonuniform, with

$$D_x(x,y,z) = D_y(x,y,z) = \frac{1}{2}(x^2+4y^2+1)(2+z), \quad D_z(x,y,z) = \frac{1}{2}(2+z),$$

for $(x,y,z) \in \overline{M}^{0}$. Finally, we take the dimensionless parameter $\epsilon = 0.01$. Recalling (2.10), this corresponds to e.g. horizontal and vertical length scales of $l = 100$ and $h = 1$ respectively, and permeability scales in the horizontal and vertical directions $D_0^H = D_0^L = 1$ respectively, all associated with the dimensional reservoir.

Example 4.1 (Single line sink, constant porosity and initial pressure). For our first example, we take the porosity and initial pressure variation to be uniform throughout the layer, with $\phi(x,y,z) = 1$ and $f(x,y,z) = 1$, for $(x,y,z) \in \overline{M}^{0}$, and we consider the case of a single line sink at $(x_1,y_1) = (0,0) \in \Omega$ with volumetric strength

$$s_1(z) = -6(z_+ - z)(z - z_-); \tag{4.1}$$

and hence $\mu_1 = -1$, $p_0 = 1$.

The computation of the remaining important quantities (meas$(\overline{M}^{0})$ (and hence I_0, in this case), A_0^1, B_j, λ_j, c_j and $\tilde{\lambda}_j$, for $j = 1,2,\ldots$) then depends on the values of the various discretisation parameters discussed in §3. In particular: our approximations to λ_j and B_j, for $j = 1,2,\ldots$, depend on the number of degrees of freedom M_{SL} used in the solution of [SL]; our approximations to meas$(\overline{M}^{0})$, A_0^1 and $\tilde{\lambda}_j$, for $j = 1,2,\ldots$, depend on the maximum side length, $\hat{h}$, of the triangles used to discretise Ω; our approximations to c_j, for $j = 1,2,\ldots$, depend on both $\hat{h}$ and on the parameter L used to define the graded mesh

	$\hat{h} = 0{:}16$	$\hat{h} = 0{:}08$	$\hat{h} = 0{:}04$	$\hat{h} = 0{:}02$	$\hat{h} = 0{:}01$
cpt(s)	$3.9\ \ 10^{0}$	$5.4\ \ 10^{0}$	$1.5\ \ 10^{1}$	$5.5\ \ 10^{1}$	$2.6\ \ 10^{2}$
N_e	69	281	1125	4527	18134
N_t	109	503	2128	8811	35779
meas($\overline{M}^{0}$)	2.3148	2.3469	2.3540	2.3556	2.3561
A_0^1	1.2398	1.2143	1.2037	1.1895	1.2036

Table 3 Computing times (in seconds), number of elements, and the dependence of meas($\overline{M}^{0}$) and A_0^1 on $\hat{h}$.

	$\hat{h} = 0{:}16$	$\hat{h} = 0{:}08$	$\hat{h} = 0{:}04$	$\hat{h} = 0{:}02$	$\hat{h} = 0{:}01$
$\tilde{\ }_1$	$4.2460\ \ 10^{+0}$	$4.3161\ \ 10^{+0}$	$4.3299\ \ 10^{+0}$	$4.3335\ \ 10^{+0}$	$4.3341\ \ 10^{+0}$
$\tilde{\ }_2$	$1.2714\ \ 10^{+1}$	$1.3199\ \ 10^{+1}$	$1.3303\ \ 10^{+1}$	$1.3327\ \ 10^{+1}$	$1.3332\ \ 10^{+1}$
$\tilde{\ }_3$	[illegible]	[illegible]	[illegible]	[illegible]	[illegible]

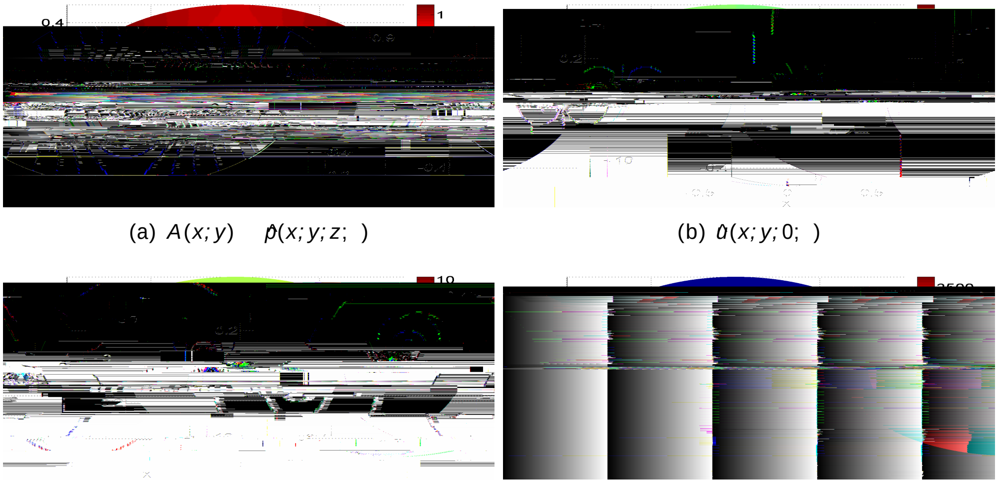

(a) $A(x,y)$ $\hat{p}(x,y,z,\ )$ (b) $\hat{u}(x,y,0,\ )$

(c) $\hat{v}(x,y,0,\ )$ (d) $\hat{w}(x,y,0,\ )$

Fig. 1 Outer region pseudo-steady state pressure and flow fields, Example 4.1.

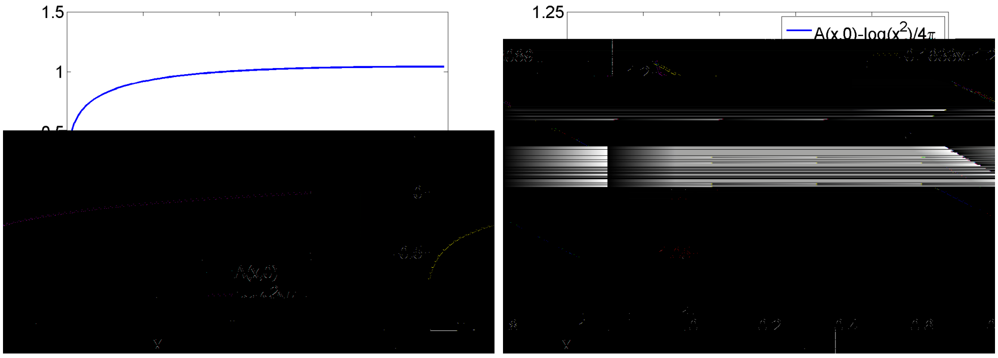

(a) Comparing $A(x,0)$ with $\log(x^2)/(4\ )$ (b) Comparing $A(x,0)$ $\log(x^2)/(4\ )$ with $0.1633x + 1.2089$

Fig. 2 Verifying equation (2.45).

a very good fit to the data, suggesting a value of the constant A_0^1 1.2089 in (4.2). This compares well with the value of $A_0^1 = 1.$.

$\hat{u}$, the y-direction, $\hat{v}$, and the z-direction, $\hat{w}$, each on a slice through $\overline{M}^0$ on the plane $z = 0$. The plots of $\hat{u}(x; y; 0; \ )$ and $\hat{v}(x; y; 0; \ )$, in Figures 1(b) and 1(c) respectively, demonstrate how the ow elds in the x and y directions are highly peaked near the line sink, and the dependence on the derivatives of $A(x; y)$ as plotted in Figure 1(a) is clear. The plot of $\hat{w}(x; y; 0; \ )$ in Figure 1(d) shows that the ow is almost entirely horizontal away from the wells, with the ow eld in the vertical direction being very highly peaked at the line sink.

In Figure 3 we plot the pseudo-steady state pressure and ow elds in the inner regions. Each of these is computed at a distance =100 from the line sink, at the point $x = y = \ =(100\sqrt{2})$, and then plotted as a function of z, the vertical coordinate. At this very small

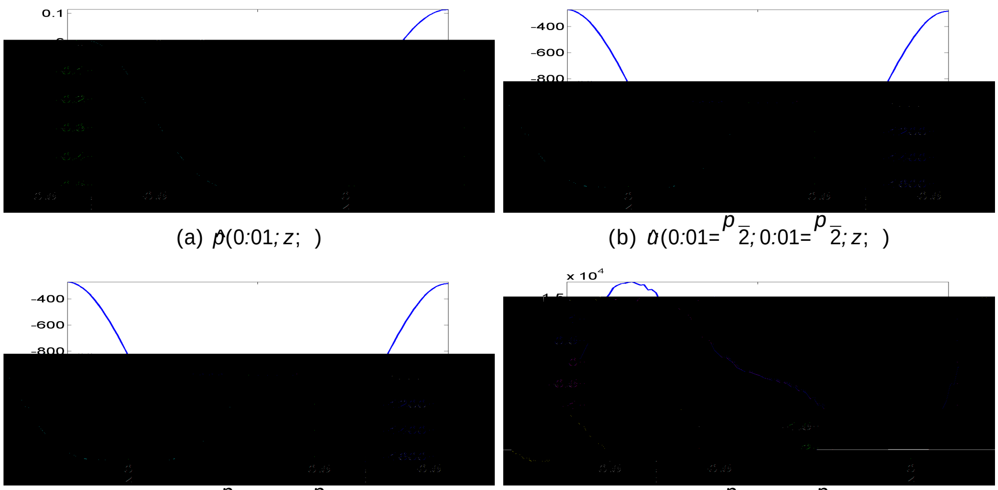

(a) $\hat{p}(0{:}01; z; \ )$ (b) $\hat{u}(0{:}01{=}\sqrt{2}; 0{:}01{=}\sqrt{2}; z; \ )$

(c) $\hat{v}(0{:}01{=}\sqrt{2}; 0{:}01{=}\sqrt{2}; z; \ )$ (d) $\hat{w}(0{:}01{=}\sqrt{2}; 0{:}01{=}\sqrt{2}; z; \ )$

Fig. 3 Inner region pseudo-steady state pressure and ow elds.

distance from the line sink, the pseudo-steady state pressure eld and the pseudo-steady state ow elds in the x and y directions each take their largest absolute values near the centre of the layer. The pseudo-steady state ow eld in the z-direction is close to zero at the upper and lower boundaries, as we would expect from the Neumann boundary conditions, but the vertical ow eld is also close to zero near the centre of the layer, positive in the lower part of the layer, and negative in the upper part of the layer, indicating that the uid is owing towards the centre of the layer at all points near the line sink. We remark that the approximation to $\hat{w}$ is piecewise constant, and at the level of graphical magni cation this is evident in Figure 3(d).

We plot our approximation to the transient pressure eld $\tilde{p}(\mathrm{r}; t)$ for $t = 1{=}400$ and $t = 0{:}1$ in Figure 4. Recalling (2.59), we note that our approximation to $\tilde{p}$ is only valid when $t \quad ^2 = 1{=}10000$. Examining the scales on the right of each of these gures, the decay of the transient pressure eld with respect to time is clear (recall (2.34) and (2.36)). Further plots for larger values of t look identical to Figure 4(b), but with $|\tilde{p}(\mathrm{r}; t)|$ decreasing (apparently uniformly) as t increases. Although the early time solution is peaked near the line sink, it

(a) $t = 1/400$ (b) $t = 0.1$

Fig. 4 Transient pressure field, $p(\mathbf{r}, t)$, computed at $t = 1/400$ and $t = 0.1$, Example 4.1.

is smooth at this point, with the singularity being captured entirely by the pseudo-steady state solution, and the evolutionary problem providing a smooth solution.

The transient flow fields in the x and y directions, $u(\mathbf{r}, t)$ and $v(\mathbf{r}, t)$ respectively, defined by (2.33) and computed at $t = 1/400$, are plotted on a slice through $z = 0$ in Figure 5. The

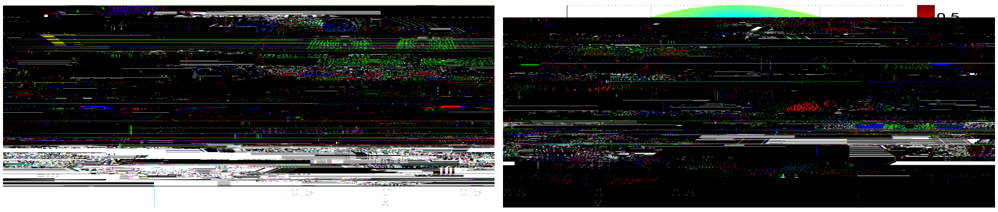

(a) $u(\mathbf{r}, t)$ (b) $v(\mathbf{r}, t)$

Fig. 5 Transient flow fields in x- and y-directions, computed at $t = 1/400$, $z = 0$, Example 4.1.

relationship between these flow fields and the corresponding transient pressure field plotted in Figure 4(a) can be clearly seen.

Example 4.2 (Change in strength of line sources/sinks). For our second example, we consider the effect of changing the strength of the single line source/sink located at $(x_1, y_1) = (0, 0)$, keeping everything else the same. In order to model a change in the line source/sink volumetric strengths, there is no need to repeat all of the calculations, particularly if the line source/sink locations are not changed. In this case we just redefine s_i, for $i = 1, \dots, N$, and then solve [IBVP] for these new line source/sink strengths, taking the final solution from the previous run as our initial data. Here, we take our initial data to be the solution from Example 4.1 at $t = 0.2$, and we halve the strength of the sink at $(x_1, y_1) = (0, 0)$ (given by (4.1) for Example 4.1), so that now

$$s_1(z) = -3(z_+^1 - z)(z - z_-^1).$$

This corresponds to halving the production rate at the well. In Figure 6 we plot the dimensional dynamic uid pressure,

$$p(x; y; 0; t^0) = Qp(x; y; 0; t) \qquad (4.3)$$

(see (6, x2) for details, recalling that Q is given by (2.9)), computed at a dimensionless distance =100 from the line sink, as for the computations of Figure 3 above, against dimensional time (t^0 = 5000t, again see (6, x2) for details) with the line sink strength having been halved at t = 0:2, corresponding to t^0 = 1000. Looking rst at the solution for

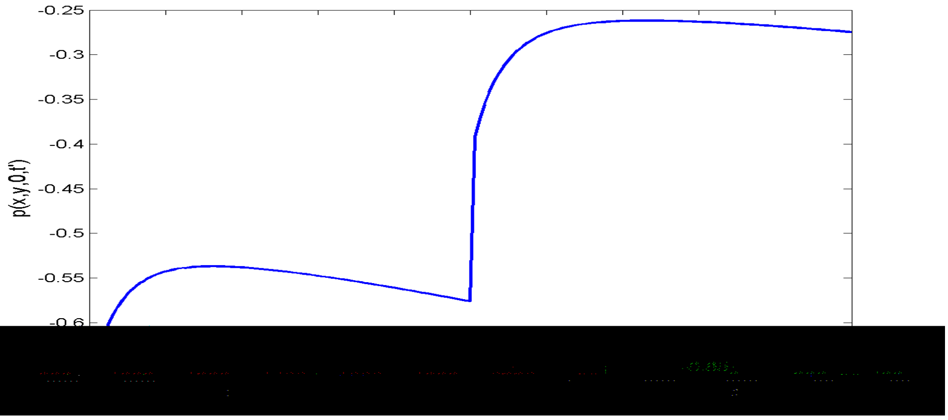

Fig. 6 Dimensional dynamic uid pressure (computed at a dimensionless distance $\epsilon/100$ from the line sink) plotted against dimensional time, with the production rate being halved at t' = 1000.

t^0 2 (0; 1000), the initial e ect of the transient eld is clear. By about t^0 = 300 this has been overtaken by the linear decay in the pressure, due to the fact that $\hat{}_T$, corresponding to the sum of the volume uxes from the line sources/sinks (recall (2.20)), is negative. At t^0 = 1000, we see the e ect of the change in production rate. The computing time required to approximate the dynamic uid pressure for t^0 2 (1000; 2000) is only 64 seconds, compared to a computing time of 260 seconds for Example 4.1 (both values correct to two signi cant sti ness matrix for the solution of both [BVP] and $[EVP]^0$ is una ected by changes to the strengths/locations of the sources/sinks. As a third example, we consider the case of three line sources/sinks, located at $(x_1; y_1) = (\ 0:5; 0)$, $(x_2; y_2$

In Figure 8 we plot the pseudo-steady state pressure and ow elds in the inner regions around each line source/sink. Each of these is computed at a distance $\epsilon/100$ from each line sink, at the point $(x - x_i) = (y - y_i) = \epsilon/(100\sqrt{2})$, for $i = 1; 2; 3$, and plotted as a function of z, the vertical coordinate. The behaviour near each line source/sink is comparable to

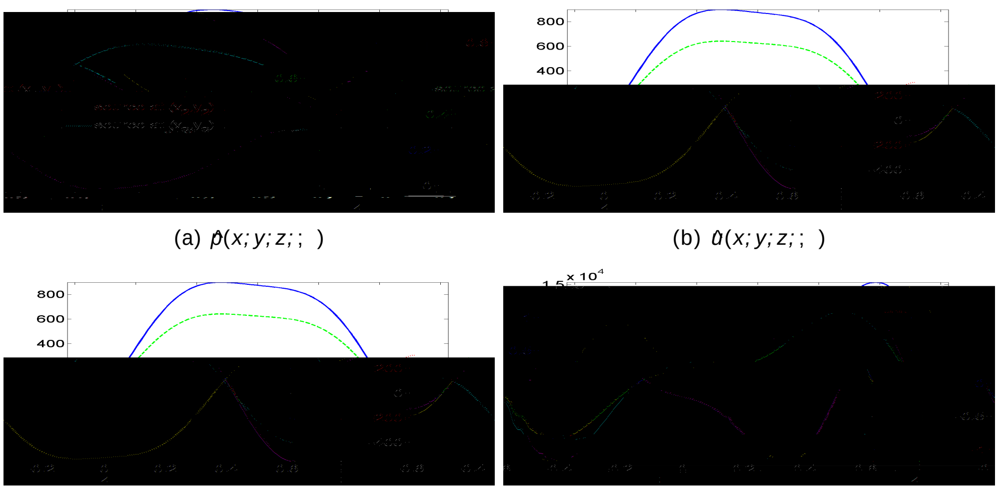

(a) $\hat{p}(x; y; z; \;)$ (b) $\hat{u}(x; y; z; \;)$

(c) $\hat{v}(x; y; z; \;)$ (d) $\hat{w}(x; y; z; \;)$

Fig. 8 Inner region pseudo-steady state pressure and ow elds, each computed at a distance $\epsilon/100$ from each source/sink. The legend is the same for each plot.

that seen in Figure 3 for Example 4.1. For the sink at $(x_3; y_3) = (0; 0{:}1)$, the vertical ow eld is positive in the lower part of the layer, and negative in the upper part of the layer, indicating that the uid is owing towards the centre of the layer at all points near the line sink. For each of the sources, the vertical ow eld is negative in the lower part of the layer,

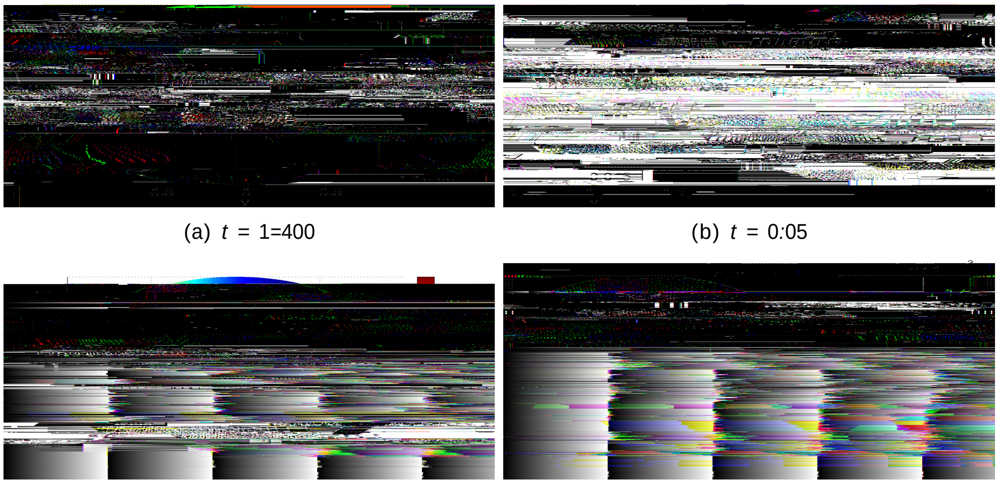

(a) $t = 1/400$ (b) $t = 0.05$

(c) $t = 0.1$ (d) $t = 0.2$

Fig. 9 Transient pressure field, $p(\mathbf{r}, t)$, computed for various t, Example 4.3.

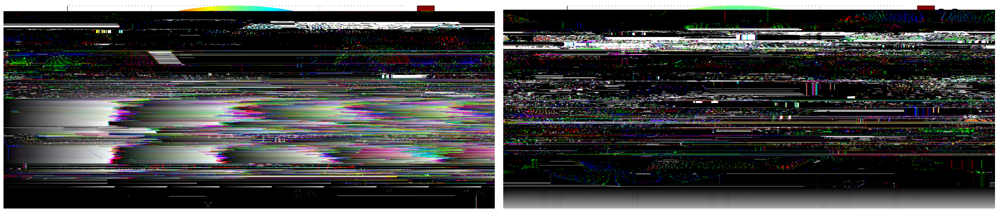

(a) $u(\mathbf{r}; t)$ (b) $v(\mathbf{r}; t)$

Fig. 10 Transient flow fields in x- and y-directions, computed at $t = 1/400$, $z = 0$, Example 4.3.

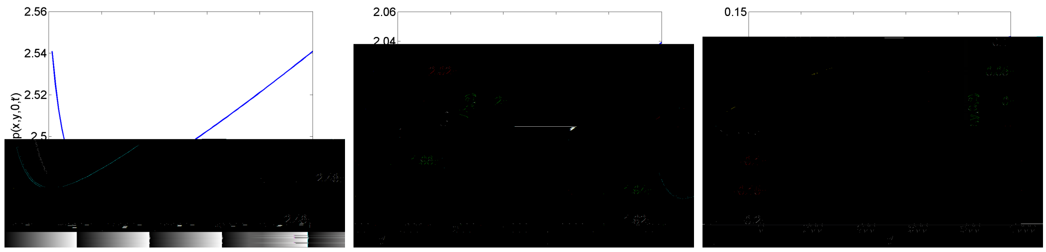

(a) source at $(x_1; y_1) = (-0.5; 0)$ (b) source at $(x_2; y_2) = (0.5; 0)$ (c) source at $(x_3; y_3) = (0; 0.1)$

Fig. 11 Dimensional pressure plotted against dimensional time, computed at a dimensionless distance $\epsilon/100$ from each line source, Example 4.3.

pressure, due to the fact that $\hat{}_T$, corresponding to the sum of the volume uxes from the line sources/sinks, is positive.

Example 4.4 (Nonuniform porosity). Finally we remark that having solved [IBVP] once, one can change certain properties of the porous layer, such as its porosity or permeability, and then recompute the solution to [IBVP] with a greatly reduced computing time, with no need to repeat calculations that are not explicitly dependent on the changed feature. To illustrate this, for our nal example, we change the porosity function so that it is no longer constant, but instead is de ned by = $(x;y;z)=$ $_0$

a weakly compressible uid in a thin porous layer. I: Two-dimensional theory. *SIAM J. Appl. Math.*, 69(4):1084{1109, 2009.

6. D. J. Needham, S. Langdon, B. A. Samson, and J. P. Gilchrist. The unsteady ow of a weakly compressible uid in a thin porous layer. II: Three-dimensional theory. Submitted for publication, University of Reading preprint MPS-2011-02, 2011.
7. V. Isakov. On inverse problems in secondary oil recovery. *European J. Appl. Math.*, 19:459{478, 2008.
8. O. Dorn and R. Villegas. History matching of petroleum reservoirs using a level set technique. *Inverse Problems*, 24(3):035015, 2008.
9. A. Friedman. *Partial Di erential Equations of Parabolic Type*. Prentice-Hall, Englewood Cli s, N.J., 1964.
10. M. Abramowitz and I. Stegun. *Handbook of Mathematical Functions*. Dover, 1972.
11. E. A. Coddington and N. Levinson. *Theory of Ordinary Di erential Equations*. McGraw-Hill Book Company, Inc., New York-Toronto-London, 1955.
12. J. Smoller. *Shock Waves and Reaction-Di usion Equations*. Springer-Verlag, Berlin, 1983.
13. G. Strang and G. J. Fix. *An Analysis of the Finite Element Method*. Prentice-Hall, Inc., Englewood Cli s, N.J., 1973.
14. O. C. Zienkiewicz and K. Morgan. *Finite Elements and Approximation*. John Wiley and Sons, Inc., 1983.
15. P.-O. Persson and G. Strang. A simple mesh generator in MATLAB. *SIAM Review*, 46:329{345, 2004.
16. D. Braess. *Finite Elements: Theory, Fast Solvers, and Applications in Solid Mechanics*. Cambridge University Press, 1997.
17. J. W. Barrett and C. M. Elliott. A practical nite element approximation of a semi-de nite Neumann problem on a curved domain. *Numer. Math.*, 51:23{36, 1987.
18. H. S. Dollar. Constraint-style preconditioners for regularized saddle point problems. *SIAM J. Matrix Anal. Appl.*, 29(2):672{684, 2007.
19. D. Huybrechs and R. Cools. On generalized Gaussian quadrature rules for singular and nearly singular integrals. *SIAM J. Numer. Anal.*, 47(1):719{739, 2008.
20. C. Schwab. Variable order composite quadrature of singular and nearly singular integrals. *Computing*, 53:173{194, 1994.